Cell Reports

Article

Signaling from Plastid Genome Stability Modulates Endoreplication and Cell Cycle during Plant Development

Graphical Abstract

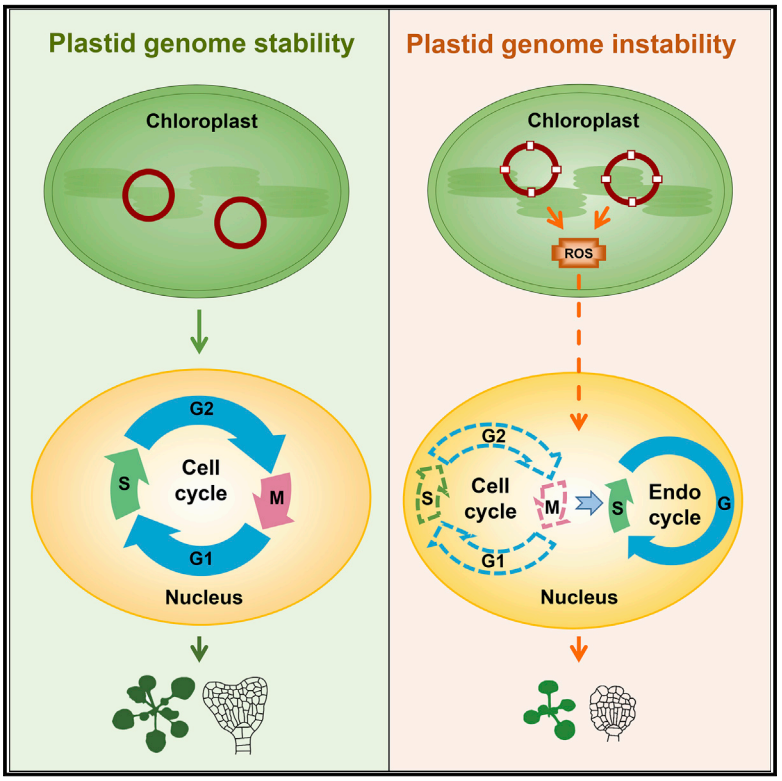

Highlights

- Plastid genome instability alters endoreplication and cell cycle
- Plastid genome instability results in increased expression of cell-cycle-related genes
- SOG1 mediates the activation of cell-cycle-related genes by plastid genome instability
- ROS is required for communication of plastid genome with endoreplication and cell cycle

Authors

Sujuan Duan, Lili Hu, Beibei Dong, Hong-Lei Jin, Hong-Bin Wang

Correspondence

jinhl@gzucm.edu.cn (H.-L.J.), wanghongbin@gzucm.edu.cn (H.-B.W.)

In Brief

Duan et al. show that plastid genome instability modulates endoreplication and cell-cycle progression by plastid-to-nucleus retrograde signaling through the SOG1-mediated pathway, which is required for plant growth and development.

Duan et al., 2020, Cell Reports *32*, 108019
August 11, 2020
https://doi.org/10.1016/j.celrep.2020.108019

CellPress

Cell Reports

CellPress
OPEN ACCESS

Article

Signaling from Plastid Genome Stability Modulates Endoreplication and Cell Cycle during Plant Development

Sujuan Duan,[1,2] Lili Hu,[1] Beibei Dong,[1] Hong-Lei Jin,[2,*] and Hong-Bin Wang[1,2,3,*]

[1]State Key Laboratory of Biocontrol and Guangdong Provincial Key Laboratory of Plant Resources, School of Life Sciences, Sun Yat-sen University, 510275 Guangzhou, People's Republic of China

[2]Institute of Medical Plant Physiology and Ecology, School of Pharmaceutical Sciences, Guangzhou University of Chinese Medicine, 510006 Guangzhou, People's Republic of China

[3]Lead Contact

*Correspondence: jinhl@gzucm.edu.cn (H.-L.J.), wanghongbin@gzucm.edu.cn (H.-B.W.)

https://doi.org/10.1016/j.celrep.2020.108019

SUMMARY

Plastid-nucleus genome coordination is crucial for plastid activity, but the mechanisms remain unclear. By treating *Arabidopsis* plants with the organellar genome-damaging agent ciprofloxacin, we found that plastid genome instability can alter endoreplication and the cell cycle. Similar results are observed in the plastid genome instability mutants of *reca1why1why3*. Cell division and embryo development are disturbed in the *reca1why1why3* mutant. Notably, *SMR5* and *SMR7* genes, which encode cell-cycle kinase inhibitors, are up-regulated in plastid genome instability plants, and the mutation of *SMR7* can restore the endoreplication and growth phenotype of *reca1why1why3* plants. Furthermore, we establish that the DNA damage response transcription factor SOG1 mediates the alteration of endoreplication and cell cycle triggered by plastid genome instability. Finally, we demonstrate that reactive oxygen species produced in plastids are important for plastid-nucleus genome coordination. Our findings uncover a molecular mechanism for the coordination of plastid and nuclear genomes during plant growth and development.

INTRODUCTION

Proper genome function depends on the maintenance of genome integrity (Aguilera and García-Muse, 2013). Plant plastids are semi-autonomous organelles containing their own genomes, encoding several proteins that are necessary for the formation of functional photosynthetic and metabolic complexes (Green, 2011). Plastid genome stability is vital for plastid function and, consequently, plant growth and development (Kimura and Sakaguchi, 2006; Oldenburg and Bendich, 2015). However, plastids are extremely sensitive to certain environmental conditions and stimuli that can damage their genome stability; in particular, double-strand breaks (DSBs) are considered the most threatening to genome instability. Spontaneously, the plastid genome-damaging agent ciprofloxacin (CIP) is a gyrase inhibitor that can also produce organellar DSBs (Evans-Roberts et al., 2016), which induce severe plastid DNA (ptDNA) rearrangements if improperly repaired (Odom et al., 2008). However, our understanding of how plants maintain plastid genome stability is limited. Several factors involved in the maintenance of plastid genome stability have been identified in *Arabidopsis thaliana*: the single-stranded DNA-binding proteins WHIRLY (WHY) 1 and WHY3 are targeted to plastids and protect the plastid genome against rearrangements (Maréchal et al., 2009); chloroplast RECA1 is key for homologous recombination (HR) and maintenance of structural integrity of the plastid genome (Rowan et al., 2010); and the type I polymerases, PolIB, perform ptDNA replication and repair in *Arabidopsis* (Parent et al., 2011). The plastid genome instability in the *Arabidopsis polibwhy1why3* triple mutant leads to the generation of reactive oxygen species (ROS) and induces stress-related nuclear genetic reprogramming, which correlates with yellow-variegated leaves and environmental stress adaption (Lepage et al., 2013). The *reca1why1why3* triple mutant, which is characterized by white variegation and a severe growth-retardation phenotype, accumulates much more short-range ptDNA rearrangements than the wild type (WT), leading to plastid genomic instability (Zampini et al., 2015), but the relationship between plastid genomic instability and plant growth remains unclear.

More than 95% of plastid proteins are encoded by the nuclear genome (Green, 2011), which contains all of the genetic information required for plastid function and plant survival (Woodson and Chory, 2008). The maintenance of nuclear genome integrity is fundamental for nuclear genome function. However, genome instability may result from failures at different steps of the DNA cycle (from replication to segregation) and failed or improper repair of DNA damage (Aguilera and García-Muse, 2013; Sanchez et al., 2012). Plants have developed an elaborate regulatory mechanism to ensure the integrity of the nuclear genome, which is required for normal growth and development (Hu et al., 2016).

Accurate control of the cell-cycle phases (G1, S, G2, and mitotic [M] phases) and critical checkpoints at G1/S, G2/M phase transition points, and metaphase (spindle assembly checkpoint [SAC]) are important for ensuring that cell division generates two identical daughter cells (De Veylder et al., 2003; Inzé and De Veylder, 2006). The checkpoint at the G1/S transition ensures that sufficiently raw materials are available for the completion of DNA replication, while the G2/M transition checkpoint ensures that cells do not initiate mitosis before repairing damaged DNA, and the SAC ensures the equal segregation of chromosomes to the daughter cells (De Veylder et al., 2003; Inzé and De Veylder, 2006). Cell-cycle progression is driven by conserved heterodimeric kinases, comprising regulatory cyclin subunits and catalytic cyclin-dependent kinase (CDK) subunits; these heterodimeric kinases are known as CDK-cyclin complexes. Plants possess different classes of CDKs and cyclins to regulate the transition from one cell-cycle phase to the next (De Veylder et al., 2003; Inzé and De Veylder, 2006). For example, A-type cyclins (CYCA) and B-type cyclins (CYCB) have a function during G1/M and G2/M phase transitions, respectively (Inzé and De Veylder, 2006; Gutierrez, 2009; Boruc et al., 2010).

Exogenous environmental factors and endogenous metabolic processes damage plant genome DNA and can lead to genomic instability. Plants have evolved a DNA damage response mechanism when DNA strands break to ensure genome integrity (Aguilera and García-Muse, 2013; Hu et al., 2016). When DNA damage is beyond repair, plants initiate cell death to avoid transmitting damaged DNA to the next generation. However, if DNA damage is minimal, then plants activate cell-cycle arrest, endoreplication, and DNA damage repair to ensure genome integrity. Cell-cycle arrest at the main surveillance checkpoints, G1/S and G2/M, allows cells to take action to tackle DNA damage (Hu et al., 2016). During endoreplication, DNA replication continues without cell division to ensure plant survival (De Veylder et al., 2011; Breuer et al., 2014). DNA repair mechanisms include mismatch repair, excision repair, and repair of DSBs via HR and nonhomologous end joining (NHEJ), and various DSB repair mechanisms have been reported in plants (Hu et al., 2016). A set of specific proteins regulate the cell cycle in response to DNA damage. For example, the NAC domain family transcription factor SOG1, a plant functional analog of animal p53, controls the expression of genes responsible for cell-cycle regulation, including cell-cycle inhibition and DNA damage responses (Ogita et al., 2018; Yoshiyama et al., 2009, 2016, 2017). The activated SOG1 directly or indirectly regulates hundreds of genes and induces a broad cascade of transcriptional responses, which control cell-cycle regulation, endoreplication, DNA repair, and cell death to ensure genome integrity (Yoshiyama et al., 2017; Adachi et al., 2011).

Given the endosymbiotic origins of plastids, the coordination of nuclear and plastid genomes is essential for ensuring eukaryotic cell integrity (Kobayashi et al., 2009). Research into both anterograde (nucleus to plastid) and retrograde (plastid to nucleus) genome communication mechanisms has focused on the coordination of gene expression between nuclear and plastid genomes, which is important for plastid function and plant growth and survival (Woodson and Chory, 2008; Chan et al., 2016). A relatively constant nuclear:plastid genome ratio is required for normal plant growth and development, so coordination of the genome state between the nucleus and plastids is required for plant survival (Golczyk et al., 2014; Li et al., 2006). However, how plants coordinate the genome-stability state between plastids and the nucleus remains unknown.

In this study, we explored the relationship between the state of the plastid and nuclear genomes. We found that plastid genome instability affects the status of the nuclear genome mediated by SOG1 through activating genes involved in enhancing endoreplication and cell-cycle regulation. We further revealed that plastid-nucleus genome communication involves increased ROS, thus controlling plant growth and development.

RESULTS

Plastid Genome Instability Modulates Endoreplication and Cell Cycle

To explore the relationship of genome status between plastid and nucleus, we introduce two plastid genome-damaging agents, including novobiocin (NOV), a gyrase inhibitor that does not induce DNA breaks or ptDNA rearrangements (Hardy and Cozzarelli, 2003), and CIP, another gyrase inhibitor that produces organellar DSBs, which induce severe ptDNA rearrangements (Evans-Roberts et al., 2016), leading to plastid genome instability (Figure 1A).

DNA content is a key characteristic for endoreplication (Breuer et al., 2014; De Veylder et al., 2011), and the expression of the cell-cycle marker gene *CYCB1;1* is important to the cell cycle in plants (Hemerly et al., 1992; Shultz et al., 2009). We treated WT plants with different concentrations of NOV, then measured the nuclear DNA content (C value). The results showed that plants did not exhibit an obvious alteration of nuclear DNA content (Figures 1B, 1C, S1A, and S1B). Furthermore, we monitored the expression of *CYCB1;1* in NOV-treated plants, and the results showed that the expression of *CYCB1;1* is also not affected (Figure 1D). When plants were treated with CIP of different concentrations, we found that the cell ploidy enhanced gradually with the increase in CIP concentration (Figures 1B, 1C, S1C, and S1D); especially when the concentration of CIP is 0.75 and 1 μM, these plants displayed decreased 2C and 4C DNA content, increased 8C and 16C DNA content, and even a 32C nuclear DNA content. Moreover, the alteration of cell ploidy of 1 μM is more significant (Figures 1E and 1F). The expression of *CYCB1;1* in a 1-μM CIP-treated plant is also significantly upregulated (Figure 1G). These results suggest that plastid genome instability with severe ptDNA rearrangements modulates endoreplication and cell-cycle progression in plants.

Endoreplication and Cell Cycle Are Altered in the *reca1why1why3* Mutant

To ensure the effect of plastid genome instability on endoreplication and cell-cycle progression, we used the *Arabidopsis* triple mutant *reca1why1why3*, which also accumulates many more short-range ptDNA rearrangements, which exhibit plastid genome instability, to further evaluate the results obtained in CIP-treated plants (Zampini et al., 2015; Figure 2A). We used five pairs of primers to examine ptDNA rearrangements and a

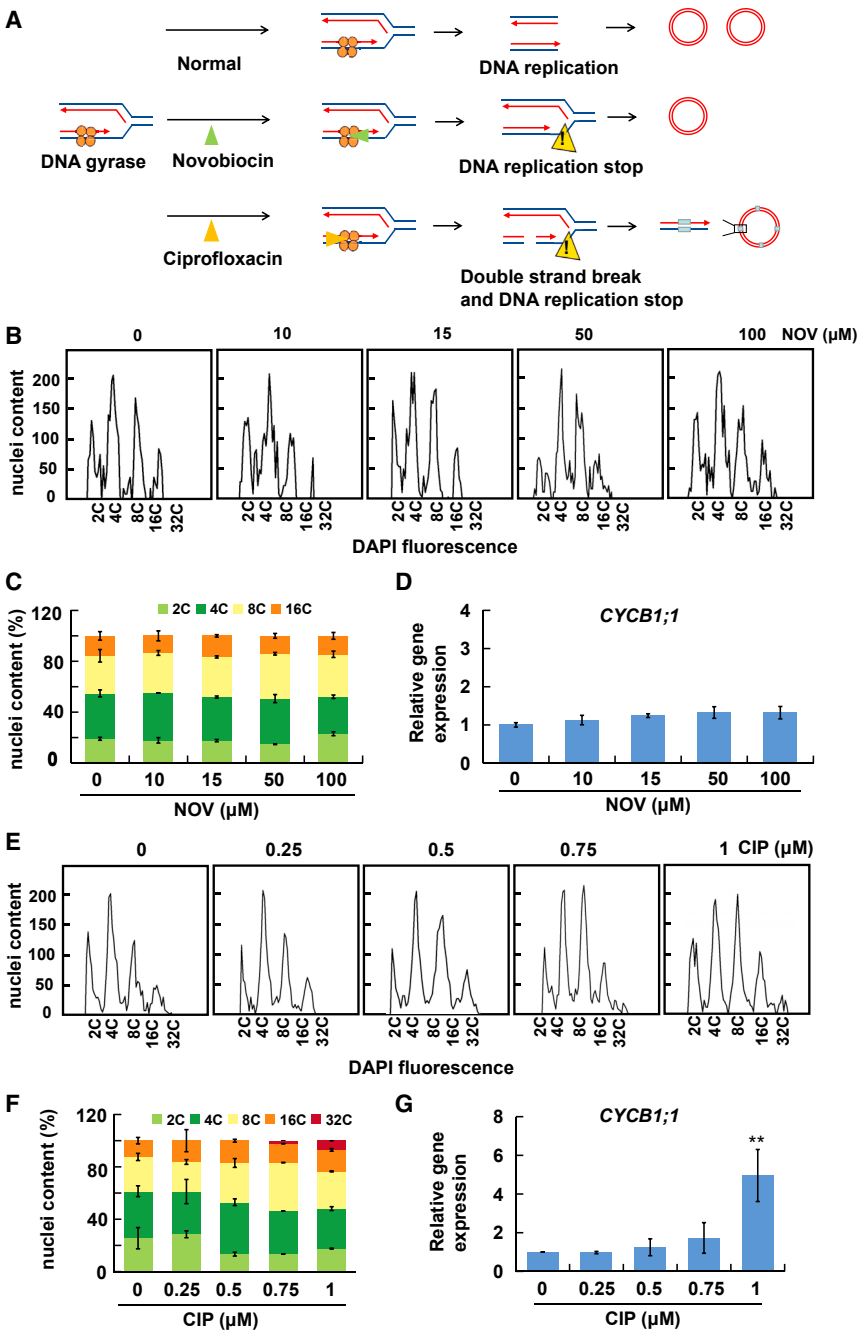

Figure 1. Analysis of the Nuclear DNA Content and Expression of *CYCB1;1* in Novobiocin (NOV)- or Ciprofloxacin (CIP)-Treated Plants

(A) Schematic representation of the function mechanism and consequence of NOV or CIP. Under the normal condition (no drug treated), the plastid genome replication is normal; under the NOV condition, the replication of ptDNA stop; and under the CIP condition, the replication of ptDNA stop and ptDNA rearrangements increased.

(B and C) Ploidy distribution (B) and nuclear DNA content (C) of 14-day-old WT or WT plants treated with NOV (10, 15, 50, and 100 μM). Three biological replicates were performed.

(D) Expression analysis of *CYCB1;1* in 14-day-old WT or WT treated with different concentrations of NOV. Three independent biological replicates were performed.

(E and F) Ploidy distribution (E) and nuclear DNA content (F) of 14-day-old WT or WT plants treated with CIP (0.25, 0.5, 0.75, and 1 μM). Three independent biological replicates were performed.

(G) Expression analysis of *CYCB1;1* in 14-day-old WT or WT treated with different concentrations of CIP. The transcript level of each gene was normalized relative to *ACTIN2* (At3g18780).

The data in (C), (D), (F), and (G) are the means ± SEs (n = 3). Three biological replicates were performed (**$p < 0.01$; Student's t test).

next-generation sequencing approach (Figure S2), referencing the previous report (Zampini et al., 2015), to ensure ptDNA instability in the *reca1why1why3* mutant. We found that nuclear DNA content in *reca1why1why3* mutants was similar to that in 1-μM CIP-treated plants (Figures 1E, 1F, 2B, and 2C) and that the expression of *CYCB1;1* is also significantly increased (Figure 2D). These results further ensured that plastid genome instability has an effect on endoreplication and cell-cycle progression.

The onset of endoreplication could be activated either by inherent developmental signals or DNA stress mostly caused by genotoxic drugs (Fox and Duronio, 2013). However, under DNA stress conditions, cells induce DNA damage responses, which contain the activation of endoreplication to maintain the integrity of the nuclear genome (Hu et al., 2016). To determine whether the DNA damage responses occurred in the *reca1why1why3* mutant, first, we ran the alkaline comet assay to examine nuclear DNA strand breaks in *reca1why1why3* mutants; the H_2O_2-treated plants were used as a control. There were no differences between the plastid genome instability plants and WT plants in this assay (Figure 2E), suggesting that there is no obvious DNA strand break in the *reca1why1why3* mutant. Second, we monitored the expression of several genes involved in various DNA repair pathways, including NHEJ (*Ku70*, *PARP2C*, and *XRCC4*) and HR (*RAD51* and *BRCA1*) (Kimura and Sakaguchi, 2006). There was almost no difference in the expression of these genes between mutants and WT plants (Figure 2F). Third, trypan blue staining to detect cell death in leaves showed no differences between mutants and WT plants (Figure 2G). These results suggest that the plastid genome instability does not directly damage nuclear DNA and trigger DNA repair, as well as cell death; instead, it affects nuclear genome status by disturbing endoreplication and cell-cycle progression.

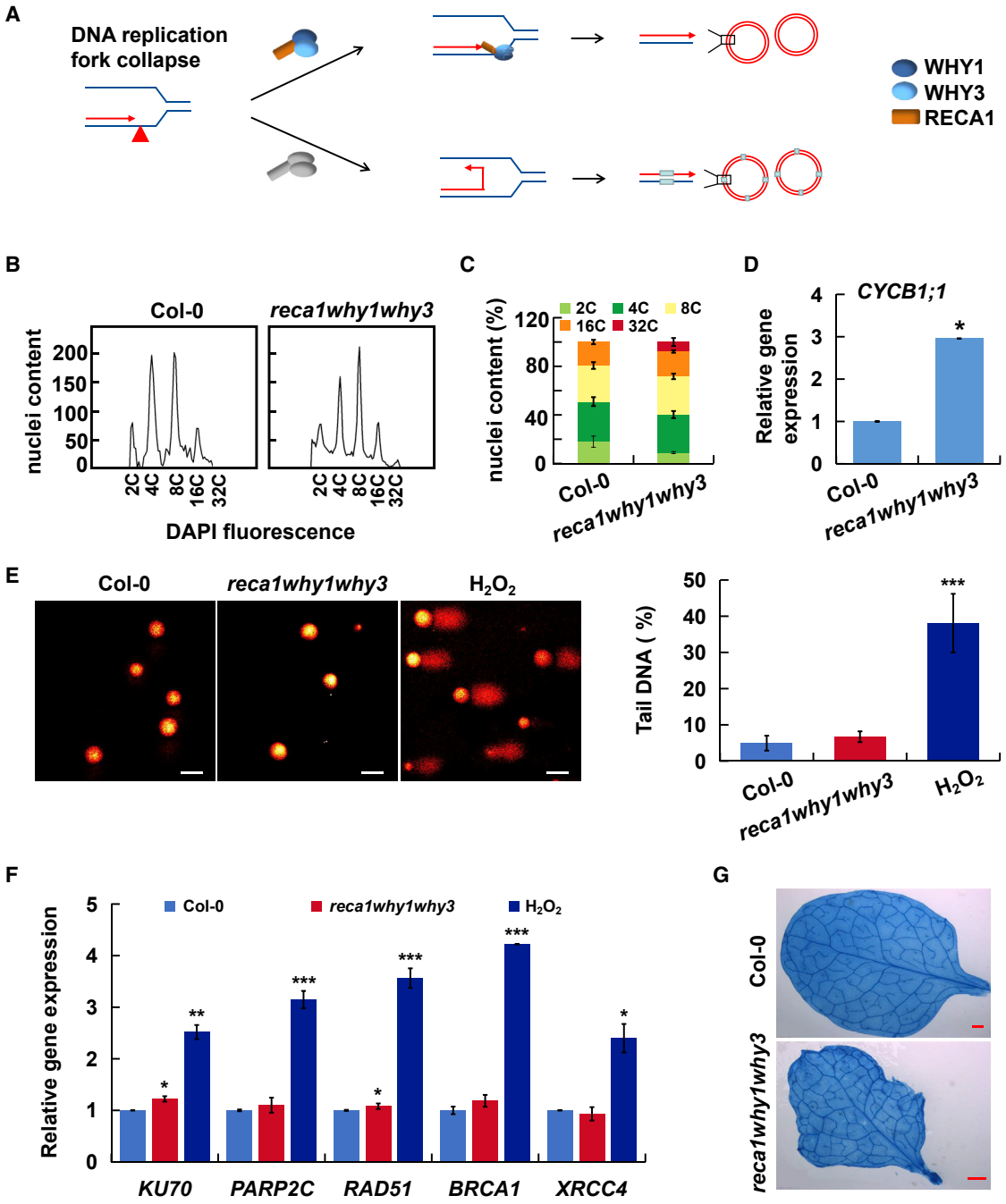

Figure 2. Nuclear DNA Content and Expression of *CYCB1;1* Are Altered in *reca1why1why3* Mutants

(A) Schematic representation of the function of plastid genome stability factors and the consequence of *reca1why1why3* mutants. In WT plants, the replication of plastid genome is normal; in *reca1why1why3* mutants, ptDNA rearrangements increased.

(B and C) Ploidy distribution (B) and nuclear DNA content (C) in 14-day-old WT and *reca1why1why3* plants. Three independent biological replicates were performed.

(D) Expression analysis of *CYCB1;1* in 14-day-old WT and *reca1why1why3* mutants. The transcript level of *CYCB1;1* was normalized relative to *ACTIN2* (At3g18780).

(E) Comet assay analysis of DNA damage status in 14-day-old WT, *reca1why1why3*-, or H_2O_2-treated plants. Scale bar, 50 μm. The statistical data for DNA in the comet tail at the right are means ± SEs (n = 60) from 3 independent biological experiments (***$p < 0.001$; Student's t test).

(F) qPCR analysis genes involved in various DNA repair pathways of 7-day-old plants. The H_2O_2-treated plants were used as the control.

(G) Representative photographs of leaves from 25-day-old plants grown under normal conditions and stained with trypan blue. Scale bar, 500 μm. Three biological replicates were performed.

The data in (C), (D), and (F) represent means ± SEs (n = 3) of 3 biological replicates, (*$p < 0.05$, **$p < 0.01$; ***$p < 0.001$; Student's t test).

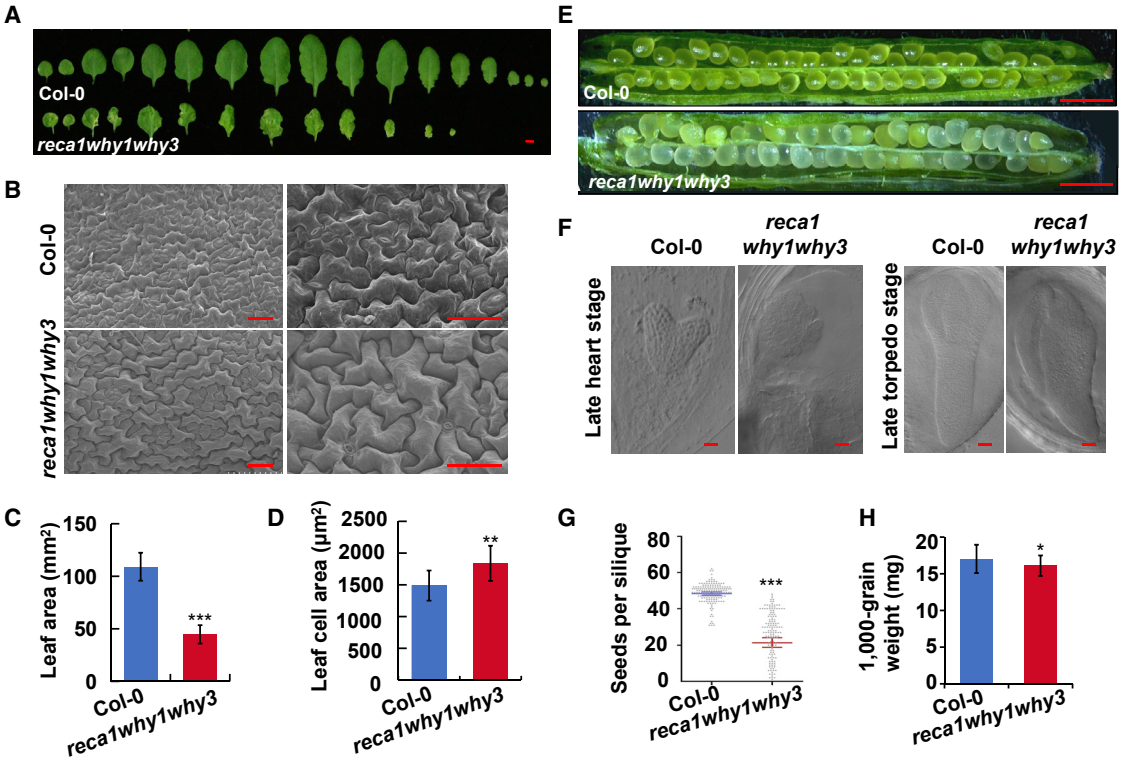

Figure 3. The Development of Leaf Cells and Embryo Development Is Affected in *reca1why1why3* Mutants

(A) Rosette leaves of WT and mutant plants ranging from the oldest (left) to the youngest (right). Scale bar, 0.5 cm.

(B) Scanning electron microscopy analysis of epidermal cells on the adaxial surface of fully differentiated leaves of 25-day-old WT and *reca1why1why3* mutants. Scale bars, 50 μm.

(C and D) Comparison of leaf area (C) and epidermal cell area (D) between WT and mutants. The data represent means ± SEs (n = 10–20 leaves) (**p < 0.01,***p < 0.001; Student's t test).

(E) Seeds of WT and mutants. Scale bar, 0.2 cm.

(F) Differential interference contrast (DIC) microscopy analysis of seeds of WT and mutants. Scale bar, 50 μm. At least 3 biological replicates were performed for each experiment.

(G) Seed fertility of WT and *reca1why1why3* plants. The data are means ± SEs (n = 140–290 siliques) of 3 biological replicates (***p < 0.001; Student's t test).

(H) Comparison of 1,000-grain weight for WT and *reca1why1why3* mutants. The data represent means ± SEs (n = 10) of 3 biological replicates (*p < 0.05; Student's t test).

Cell Division and Embryo Development Are Disturbed in the *reca1why1why3* Mutant

To explore how plastid genome instability modulates the endoreplication and cell cycle, we analyzed the growth and development of the *reca1why1why3* mutants. The mutants display a dwarf phenotype; the average leaf size in *reca1why1why3* mutants was 3.01-fold smaller than that in WT plants (Figures 3A and 3C). However, the average leaf epidermal cell area was 1.46-fold larger in the *reca1why1why3* mutants compared with that in the WT (Figures 3B and 3D). This suggested that cell division was severely inhibited in *reca1why1why3* plants.

In *Arabidopsis*, several cell-cycle-related mutants exhibit defective embryo development, even causing embryo lethality and reduced silique fertility (Domenichini et al., 2012; Ni et al., 2009). At the reproductive stage, *reca1why1why3* mutant siliques contained a large number of white ovules, in contrast to the green ovules of the WT (Figure 3E). We examined ovule development and found that *reca1why1why3* mutant embryos displayed an abnormal shape at the late heart stage and late torpedo stage compared with the WT embryo (Figure 3F). Moreover, mutant plants exhibited lower fertility than WT plants, with significantly fewer seeds per silique in the mutant (mean value of 26.0) than in the WT (mean value of 48.7) (Figure 3G). In addition, the 1,000-grain weight was lower in *reca1why1why3* than that in WT plants (Figure 3H). These results indicate that embryo development is disturbed in *reca1why1why3* mutants. In all, abnormal development of leaves and embryos in the *reca1why1why3* mutant was likely caused by defects in cell division and the cell cycle, which further supported that plastid genome instability modulates endoreplication and cell-cycle progression.

Cell-Cycle Kinase Inhibitors SMR5 and SMR7 Are Required for Regulation of Endoreplication and Cell Cycle by Plastid Genome Instability

To understand the molecular mechanisms underlying the endoreplication and cell-cycle progression in plastid genome instability plants, we performed reverse-transcriptase-quantitative PCR (RT-qPCR) to determine the expression levels of

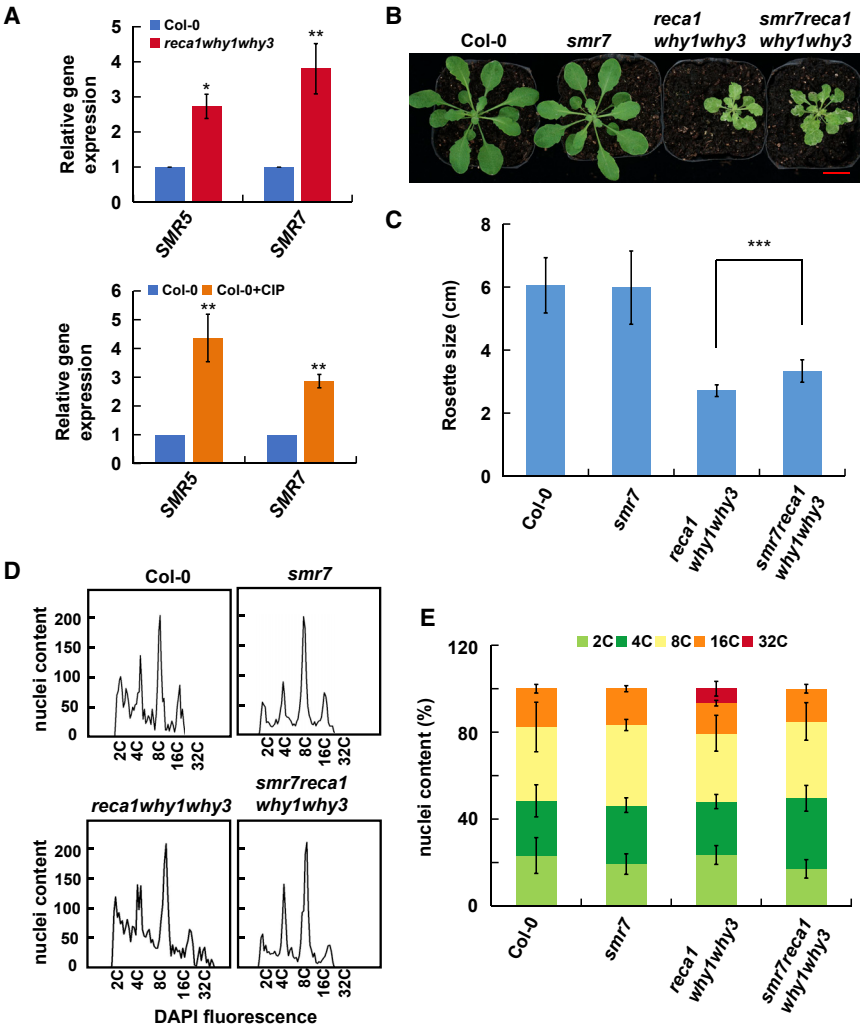

Figure 4. Expression of Cell Cycle Genes Is Enhanced in *reca1why1why3* Mutants

(A) Expression analysis of *SMR5* and *SMR7* in WT, *reca1why1why3* mutants, and CIP-treated plants. The transcript level of each gene was normalized relative to *ACTIN2* (At3g18780). The data represent means ± SEs (n = 3) of 3 biological replicates. (B–E) The phenotype (B), rosette size (C), ploidy distribution (D), and nuclear DNA content (E) of 25-day-old WT, *smr7*, *reca1why1why3,* and the quadruple of *smr7reca1why1why3* plants. The quadruple plants were isolated from an F4 segregating population generated by crossing *reca1-why1why3* with *smr7*. The graph of (C) represent means ± SEs (n = 30). (B) Scale bar, 2 cm. Three biological replicates were performed for each experiment. Asterisks indicate significant differences in (A) and (C) (*p < 0.05; **p < 0.01; ***p < 0.001; Student's t test).

cell-cycle-related marker genes during different phases: G1 (*CYCD3;3* and *SMR6*), G1/S (*KRP2, E2FA*, and *FBL17*), S (*CYCD3;1*, *CYCD5;1*, *CDT1A*, *ASF1a*, *ASF1b*, and *ETG1*), S/G2 (*CYCA2;1* and *WEE1*), and G2/M (*SMR5, SMR7*, *CCS52A1*, and *CCS52A2*) (Boruc et al., 2010; Gutierrez, 2009). Transcript levels of the SIAMESE-RELATED kinase inhibitors *SMR5* and *SMR7* were significantly increased in *reca1why1why3* mutants and CIP-treated plants (Figure 4A). Genes associated with other phases were not obviously altered (Figures S3A and S3B). These results suggested that the alteration of cell-cycle progression in plastid genome instability plants is probably due to the increased expression of cell-cycle genes.

To further determine the function of these altered cell-cycle-related genes in plastid genome instability plants, we crossed the cell-cycle gene mutant of *smr7* with the *reca1why1why3* mutant and obtained the quadruple mutant *smr7reca1why1-why3* (Figures 4B, 4C, and S3C). The growth phenotype of the quadruple mutants was partially recovered to that of the WT plants (Figures 4B and 4C). The obvious 32C nuclear DNA content was not seen in these quadruple mutants, and the DNA content recovered to the WT-like pattern in these quadruple mutants (Figures 4D and 4E). These results suggest that high expression levels of *SMR5* and *SMR7* are responsible for enhanced endoreplication and cell-cycle progression, as well as plant development in plastid genome instability mutants.

To verify the relationship of the endoreplication and cell cycle with plastid genome-stability factors, we examined the expression of cell-cycle-related marker genes and endoreplication in *reca1-1, why1*, and *why3* single mutants (Maréchal et al., 2009; Rowan et al., 2010). There were no significant differences in the expression of cell-cycle-related genes among the single mutants and WT plants (Figure S4A). Similarly, cell ploidy was the same in the single mutants (*reca1-1, why1*, or *why3*) as it was in WT plants (Figures S4B and S4C). Thus, it is possible that plastid genome instability in the single mutants is not severe enough to cause changes in endoreplication and the cell cycle.

SOG1 Is Important for Activation of Cell-Cycle-Related Genes by Plastid Genome Instability

The transcription factor of SOG1 directly controls the genes responsible for cell-cycle regulation, such as CDK inhibitors (Yi et al., 2014, Ogita et al., 2018). To determine whether the cell-cycle genes *CYCB1;1*, *SMR5*, and *SMR7* were directly regulated by SOG1 in plastid genome instability plants, we ruled out differences in the transcription levels of *SOG1* between mutants and WT plants (Figures S3A and S3B). Next, chromatin immunoprecipitation (ChIP) assays, followed by qPCR analyses indicated that the binding rates of SOG1 with *CYCB1;1*, *SMR5*, and *SMR7* were greater in *reca1why1why3* mutants (Figure 5A). Lastly, we treated the *sog1* mutants with CIP to mimic the quadruple *sog1reca1why1why3* mutants (Figure S3E). CIP is used to determine the roles of SOG1 in plastid genome instability

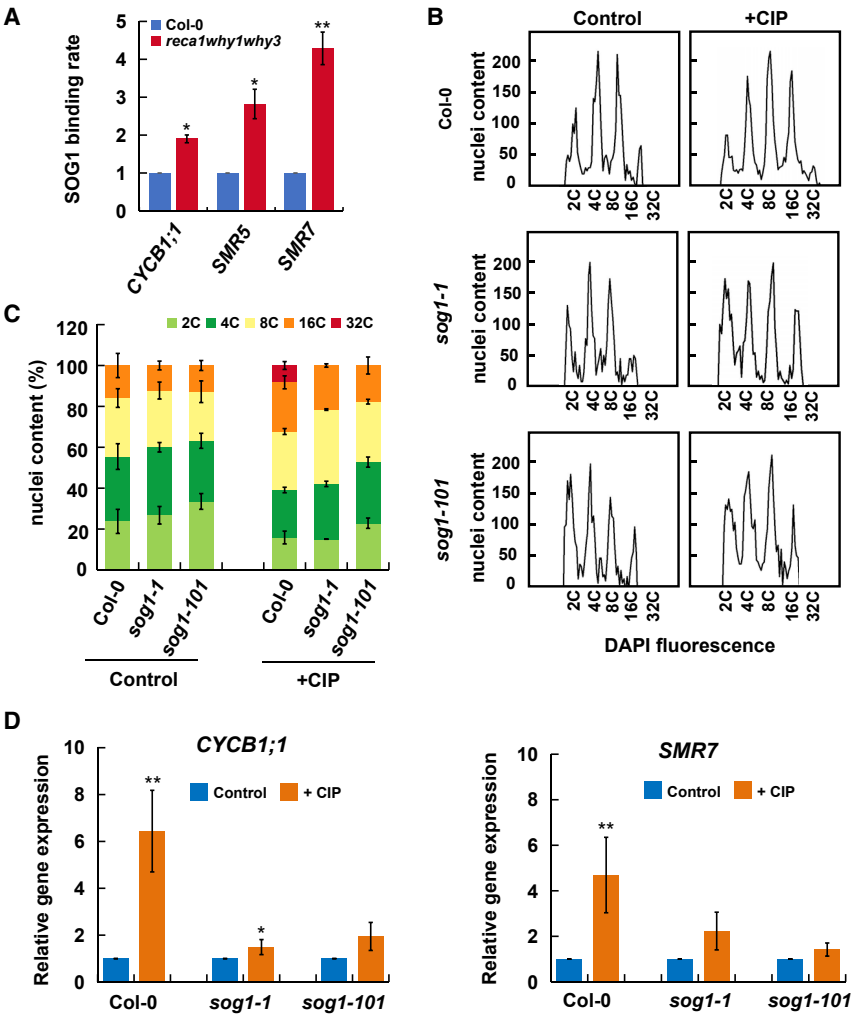

Figure 5. The Roles of SOG1 in Modulation of Cell Ploidy and Expression of Cell-Cycle-Related Genes Triggered by Plastid Genome Instability

(A) ChIP-qPCR analyzed the binding of SOG1 to the promoter regions of *CYCB1;1*, *SMR5*, and *SMR7* in *reca1why1why3* mutants compared to WT plants. The data represent means ± SEs (n = 3); 3 biological replicates were performed.

(B and C) Ploidy distribution (B) and nuclear DNA content (C) of 14-day-old WT, *sog1-1*, and *sog1-101* plants treated with or without CIP. Three biological replicates were performed.

(D) Expression analysis of *CYCB1;1* and *SMR7* in 14-day-old WT, *sog1-1*, and *sog1-101* plants treated with or without CIP. The transcript level of each gene was normalized relative to *ACTIN2* (At3g18780). The data represent means ± SEs (n = 3) of 3 biological replicates.

For (A) and (D), asterisks indicate significant differences (*$p < 0.05$; **$p < 0.01$; Student's t test).

plants. The result showed that the decreased 2C and 4C DNA content and the increased 8C, 16C, and 32C nuclear DNA content were recovered in *sog1* mutants compared with Col-0 after CIP treatment. The high expression of these cell-cycle genes induced by treatment with CIP was suppressed in *sog1* mutants (Figures 5B–5D). These results suggest that SOG1 plays vital roles in regulating endoreplication and the expression of cell-cycle genes in *reca1why1why3* mutants.

ROS Play Roles in Communication of Plastid Genome Instability with Endoreplication and Cell Cycle

We investigated whether nuclear function in the *reca1why1why3* mutant was altered through plastid retrograde signaling. Chlorophyll is synthesized via the tetrapyrrole pathway, and the intermediates of tetrapyrrole biosynthesis are thought to participate in plastid-nucleus communication in both *Chlamydomonas* and plants (Chi et al., 2013; Chan et al., 2016). The total chlorophyll *a* and *b* contents were lower in *reca1why1why3* than in WT plants (Figure S5A). Using the *gun5* mutant (*GUN5* encodes the H-subunit of Mg-chelatase) (Chan et al., 2016; Woodson et al., 2011), we examined the expression of cell-cycle-related genes in the CIP-treated *gun5* mutant to determine whether tetrapyrrole pathway intermediates participate in plastid-nucleus transmission in plastid genome instability plants. There were no differences in the expression of cell-cycle genes between *gun5* and WT plants treated with or without CIP (Figure S5B), suggesting that tetrapyrrole pathway intermediates are not involved in plastid-to-nucleus signal transmission in plastid genome instability plants.

Notably, ROS can act as important signaling messengers, which play important roles in many biotic and abiotic stress responses (Chi et al., 2013; Chan et al., 2016). To explore whether the ROS play a role in plastid genome instability plants, we determined whether ROS are induced in *reca1why1why3* mutants. Nitro blue tetrazolium (NBT) staining for O_2^- and diaminobenzidine (DAB) staining for H_2O_2 in growth light (GL, 100 μmol photons m^{-2} s^{-1}) conditions of triple mutant and WT plants demonstrated greater accumulations of ROS in *reca1why1why3* mutants (Figure 6A). We then detected the subcellular localization of ROS by the fluorescence dye staining of CM-H_2DCFDA. The result showed that the ROS colocalized with a plastid nucleoid protein, PEND, partially in the *reca1why1why3* mutants and CIP-treated plants (Terasawa and Sato, 2005; Wang et al., 2014; Figure S5C), which suggested that ROS mostly accumulated in the plastids of plastid genome instability plants.

Plants depend on light energy for photosynthesis, but excess light can cause oxidative damage and produce ROS, which can damage the photosystem conversely to inhibit photosynthesis (Rossel, et al., 2007; Li et al., 2009; Roach and Krieger-Liszkay, 2014). We checked the light-response curves of the photosystem II (PSII) quantum yield (Φ_{PSII}) and the electron transport rate (ETR) in *reca1why1why3* plants to determine the photosynthetic activity under the GL condition. When actinic light intensity

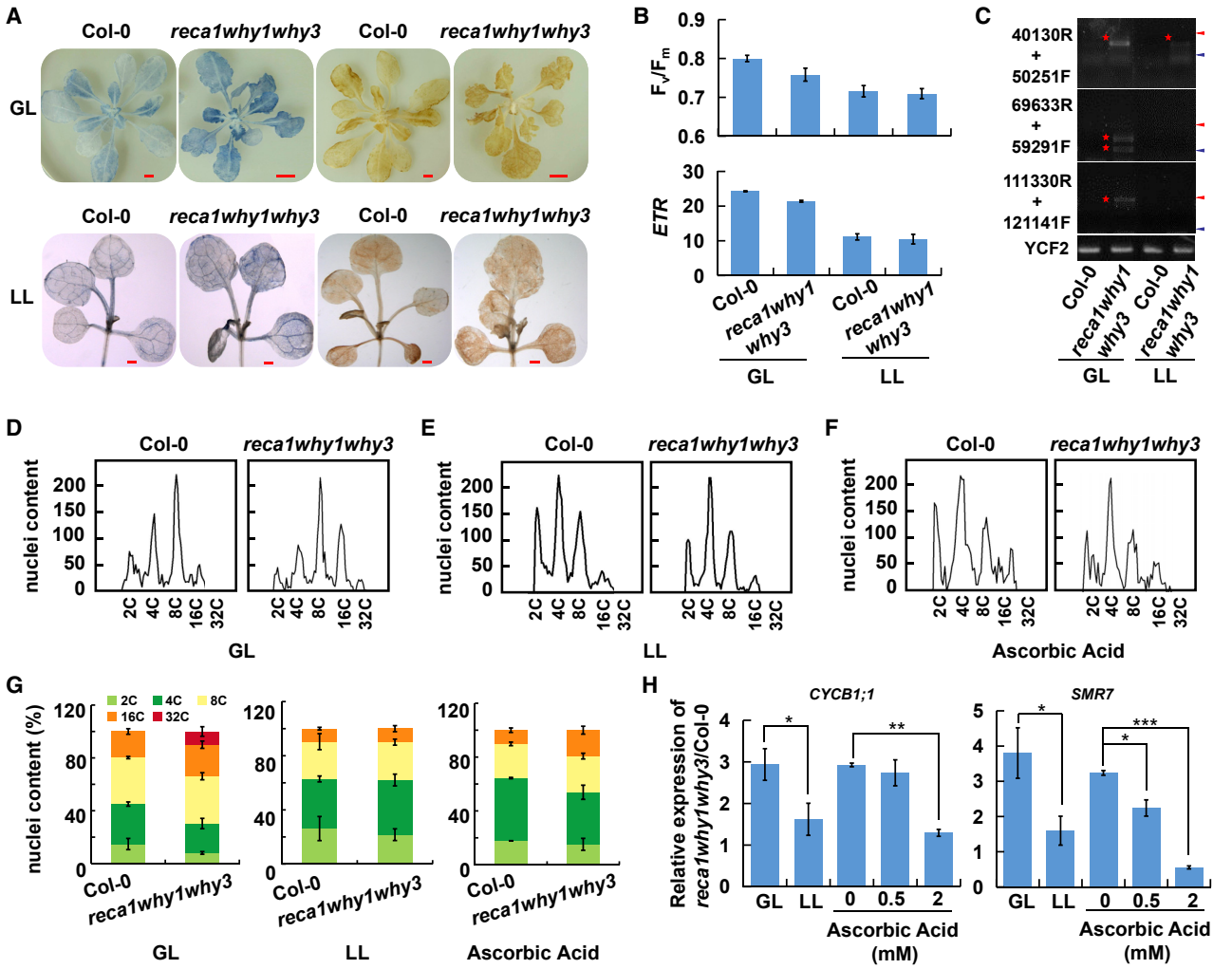

Figure 6. Production of Reactive Oxygen Species (ROS) in *reca1why1why3* Mutant Affects the Nuclear DNA Contents and Expression of Cell-Cycle-Related Genes

(A) NBT staining (left 2 panels) for O^{2-} and DAB staining (right 2 panels) for H_2O_2 in 25-day-old WT and *reca1why1why3* mutant plants grown under GL and LL conditions (scale bars: GL, 0.5 cm; LL, 500 μm). Two additional independent biological replicates were performed with similar results.

(B) The F_v/F_m and ETR in 25-day-old WT and *reca1why1why3* plants grown under GL and LL conditions. Five biological replicates were performed.

(C) ptDNA rearrangements in 25-day-old WT and *reca1why1why3* plants grown under GL and LL conditions; the red asterisks indicate the increased ptDNA rearrangements in *reca1why1why3* plants. The red and blue arrows represent DNA marker sizes of 2,000 and 750 bp, respectively. Three independent biological replicates were performed, and irrelevant lanes between GL and LL from 1 gel are eliminated.

(D–G) Analysis of ploidy distribution (D–F) and nuclear DNA content (G) in 25-day-old *reca1why1why3* mutant and WT plants under GL (D) or LL (E), or ascorbic acid-treated plants (F). Three independent biological replicates were performed, with similar results.

(H) Expression of *CYCB1;1* and *SMR7* in 25-day-old *reca1why1why3* mutants and WT plants under LL conditions or 14-day-old *reca1why1why3* mutant and WT seedlings grown on plates with increasing concentrations of ascorbic acid (a ROS quencher, 0.5 and 2 mM). The data represent means ± SEs (n = 3) of 3 biological replicates. Asterisks indicate significant differences (*$p < 0.05$; **$p < 0.01$; ***$p < 0.001$; Student's t test).

increased, the Φ_{PSII} and ETR values appeared to be lower in *reca1why1why3* plants than that in WT plants (Figure S6A), indicating that PET is affected in the *reca1why1why3* mutant. NBT and DAB staining of *reca1why1why3* mutants and WT plants under low light (LL, 10 μmol photons m^{-2} s^{-1}) conditions showed that the excess of ROS accumulation in *reca1why1why3* mutants is decreased greatly in contrast to GL conditions (Figure 6A). We then examined the photosynthetic efficiency of *reca1why1why3* in both GL and LL conditions and measured the maximum photochemical efficiency of PSII (F_v/F_m) and ETR, the minimum fluorescence (F_o), the maximum fluorescence (F_m), nonphotochemical quenching (NPQ), and photochemical quenching (qP) (Figures 6B, S6B, and S6C). The values of F_v/F_m and ETR were lower in the mutant than in WT under GL conditions, but under LL conditions, the difference in F_v/F_m and ETR between *reca1why1why3* and WT plants diminished (Figure 6B). We further examined the ptDNA rearrangements in both light conditions and found that ptDNA rearrangements in

reca1why1why3 were greatly reduced under LL conditions compared with that in GL conditions (Figure 6C). Moreover, the retarded growth phenotype of *reca1why1why3* compared with the WT was alleviated under LL conditions (Figure S6C), indicating that LL can decrease ROS and ptDNA rearrangements, which alleviate the differences in photosynthetic activity and plant growth of *reca1why1why3* mutants.

To explore the relationship between ROS accumulation and the altered endoreplication and cell cycle in *reca1why1why3*, we examined the DNA contents and expression of cell-cycle genes under LL conditions. Results showed the high DNA contents and upregulation of the cell-cycle genes of the *reca1why1why3* mutant were diminished under LL conditions (Figures 6D, 6E, 6G, and 6H). To further confirm this, we treated *reca1why1why3* mutants with ascorbic acid, a ROS quencher (Petrillo et al., 2014). Similarly, cell ploidy and the expression of cell-cycle genes in *reca1why1why3* mutants were almost reduced to the level observed in the WT at 2 mM ascorbic acid (Figures 6F–6H), supporting the idea that ROS play roles in the enhanced endoreplication and expression of cell-cycle-related genes in *reca1why1why3* mutants.

To examine whether reduced photosynthesis in *reca1why1why3* mutants contributes to endoreplication and cell-cycle progression in the nucleus, we introduced a photosynthesis-defected mutant *lpe1-3*, which specifically affects PSII activity drastically (Jin et al., 2018), as a control. As we can see, the Φ_{PSII} and ETR photosynthetic efficiency in the *lpe1-3* mutant were severely reduced (Figures S6A and S6B). The *lpe1-3* mutants exhibit severe growth retardation, which is similar in the phenotype of *reca1why1why3* mutants, so we measured leaf size, leaf cell area, and cell number in the mutants of *lpe1-3*. The average leaf size was 5.52-fold smaller in *lpe1-3* plants than in the WT, and the average cell area in *lpe1-3* plants was similar to that in WT plants (Figure S6D). The cellular cause for reduced leaf size in *lpe1-3* was a reduction in cell number (Figure S6D), suggesting that cell division is not altered in *lpe1-3* mutants. Furthermore, plant ploidy and expression of cell-cycle genes exhibited no differences from those in WT (Figures S6E and S6F), suggesting that only the decrease in photosynthesis did not contribute to endoreplication and cell-cycle progression in the nucleus.

DISCUSSION

The stability of plastid and nuclear genomes and their interaction or communication is extremely important for plastid function and plant growth and development. However, coordination between plastid and nuclear genome status in plants is not well understood. Here, we demonstrated that plastid genome instability modulates nuclear genome status by modulating endoreplication and cell-cycle progression (Figure 7).

We provided several lines of evidence to support the notion that plastid genome instability affects endoreplication and cell-cycle progression. Plastid genome instability induced by the plastid genome-damaging agent CIP (Evans-Roberts et al., 2016) alters endoreplication and the cell cycle (Figure 1). Then, plastid genome instability mutant *reca1why1why3* shows a similar enhanced cell cycle and endoreplication to CIP-treated plants, which is supported by abnormal cell division and embryo development (Figure 3). Furthermore, we did not observe changes in the cell cycle or endoreplication or the growth defect phenotype in the plastid genome instability single mutants *why1, why3*, and *reca1-1* (Figure S4; Maréchal et al., 2009; Rowan et al., 2010). The plastid genome in these single mutants is not severely damaged, and the main difference between *reca1why1why3* mutant and single mutants is that the *reca1why1why3* mutant accumulates many more short-range ptDNA rearrangements (Zampini et al., 2015). In addition, cell cycle, cell division, and cell ploidy are not altered in the photosynthesis-defected mutant *lpe1-3* (Figures S6D–S6F), suggesting that only the decrease in photosynthesis did not contribute to endoreplication and cell-cycle progression. However, it is also possible that there is an effect of cell-cycle progression induced by growth and development on endoreplication due to the phenotype difference between the *reca1why1why3* mutant and WT plants.

In the red alga *Cyanidioschyzon merolae,* plastid organelle DNA replication is coordinated with nuclear DNA replication (NDR) during the G1/S phase transition through the Mg-protoIX signal, which is conserved in higher plants, as revealed by analyzing plant cell suspension cultures (Kobayashi et al., 2009, 2011). A previous study reported that chloroplast dysfunction likely influences cell-cycle progression (Hudik et al., 2014), but the molecular mechanism is unclear. Our study found that the expression of *SMR5* and *SMR7* is increased in plastid genome instability plants. Mutation of the cell-cycle kinase inhibitor in *reca1why1why3* partially restores the changed cell division, endoreplication, and rosette size triggered by plastid genome instability (Figure 4), which is consistent with their function in previous reports (Kumar et al., 2015; Pedroza-García., 2017; Yi et al., 2014; Churchman et al., 2006), suggesting that *SMR5* and *SMR7* is required for the alteration of endoreplication and cell cycle triggered by plastid genome instability. The cell-cycle genes *SMR5* and *SMR7* can inhibit the activity of CDKs (such as CDKB, which is required for G2/M phase and regulates the transition from the mitotic cell cycle to endoreplication) (Kumar et al., 2015; Pedroza-García, 2017; Churchman et al., 2006). The expression of G2/M phase-specific genes *CDKB1;2* was significantly decreased, and the gene expression for endoreplication, including *CCS52A2*, *SIM*, and *SMR1*, was slightly increased in CIP-treated plants (Figure S1E), further supporting that endoreplication is increased in plastid genome instability plants. Therefore, it is possible that plastid genome instability alters the cell cycle by disturbing G2/M phase to promote the endoreplication. In addition, a previous study reported that *SMR* genes can be activated in the DNA stress response (Yi et al., 2014). CDKB1 and CYCB1 mediate HR during DNA damage and form active complexes that can phosphorylate RAD51 *in vitro* (Weimer et al., 2016). Expression of the cell-cycle gene *CYCB1;1* was obviously increased; however, the magnitude of the increased expression of DNA repair marker genes *RAD51* and *KU70* was small in *reca1why1why3* mutants (1.08-fold and 1.21-fold, respectively) (Figures 2D and 2F), compared with previous reports (~2- to 50-fold, depending on the mutants or DNA stress treatment) (Domenichini et al., 2012; Horvath et al., 2017). Moreover, the alkaline comet assay revealed no obvious nuclear DNA strand breaks in *reca1why1why3* plants, implying that the effect of plastid genome instability on nuclear DNA damage is

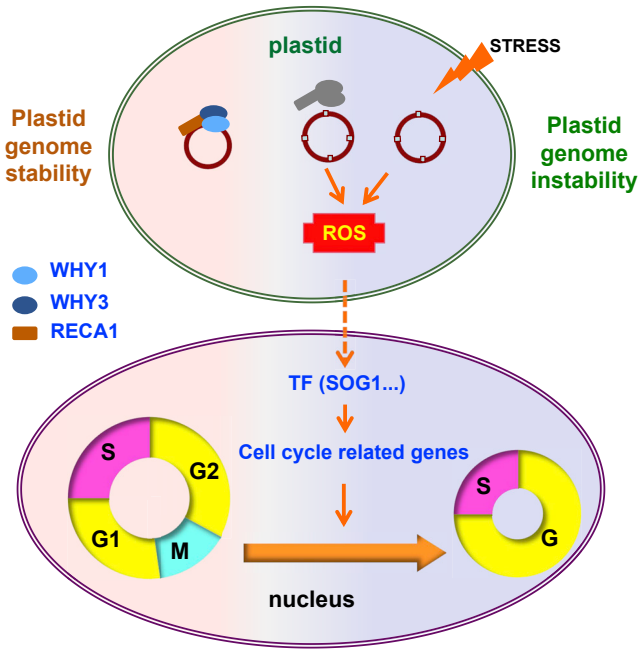

Figure 7. Proposed Model Showing the Coordination between Plastid Genomes and Nuclear Genomes for the Promotion of Plant Growth and Development

Plastid genome instability, caused by the mutation of RECA1, WHY1, and WHY3 or by external stress (e.g., CIP), promotes the accumulation of ROS, which are transmitted to the nucleus to regulate the expression of cell-cycle-related genes. The promoters of these genes are bound by SOG1 or other transcription factors. Regulation of cell-cycle progression and endoreplication, which ultimately affects plant growth and development.

mild (Figure 2E). Previous studies reported that the activation of *CYCB1;1* could also be a result of the longer arrest of cells in G2/M phase (Ni et al., 2009; Hudik et al., 2014; Yin et al., 2009). Thus, it is possible that higher expression levels of *CYCB1;1* in plastid genome instability plants also result from the longer arrest of cells in the G2/M phase, which is supported by the higher expression of *SMR7* and recovery of the cell cycle by SMR deficiency in *reca1why1why3* plants (Figures 1G, 2D, and 4). We speculate that the high expression levels of *SMR5* and *SMR7* genes contribute to the prolongation of the cell cycle of G2/M phase, and promote endoreplication instead of cell division in the *reca1why1why3* mutant.

Notably, the transcription factor of SOG1 is required for the expression of cell-cycle-related genes in different conditions (Yi et al., 2014, Ogita et al., 2018). This study showed that the increase in cell-cycle-related genes, including *SMR5*, *SMR7*, and *CYCB1;1* in the *reca1why1why3* mutant, also depends on SOG1 (Figure 5). However, in CIP-treated *sog1* plants, the deficiency of SOG1 did not fully complement the DNA ploidy or the expression levels of *CYCB1;1* and *SMR7* to those of the WT (Figures 5B–5D), suggesting that there are perhaps other transcription factors with functions similar to SOG1. Previous studies reported that DNA stress-inducing conditions promote the phosphorylation of SOG1, and the phosphorylated SOG1 activates various responses to DNA damage, such as altering the expression of cell-cycle genes to modulate cell-cycle progression (Chen et al., 2019; Yoshiyama, 2016; Yoshiyama et al., 2017). Our results suggest that SOG1 can also mediate the signaling from plastid genome instability to regulate the expression of cell-cycle genes (Figure 5). Previous studies reported that the activation of SOG1 is mediated by two kinases, ataxia-telangiectasia mutated (ATM) and ATM- and Rad3-related (ATR), which is in response to ROS in the nucleus (Yoshiyama et al., 2009, 2013; Sjogren et al., 2015). We further found that plastid genome instability promotes ROS production in plastids (Figures 6A–6C), combined with previous studies (Hudik et al., 2014; Pedroza-García et al., 2016), suggesting that SOG1 probably can also sense the signal of plastid genome instability through the ROS, besides DNA damage in the nucleus.

Traditional plastid retrograde signals originate from plastids, including intermediates of tetrapyrrole biosynthesis, PGE, the redox state, ROS, and some metabolites (Chi et al., 2013; Chan et al., 2016). In addition, defects in plastid protein import (Kakizaki et al., 2009), plastid division (Šimková et al., 2012), and tocopherols in plastids (Fang et al., 2018) suggest that more plastid functions may initiate plastid-to-nucleus retrograde signaling. Our study suggests that the ptDNA rearrangements act as a signal source associated with ROS accumulation, which modulates endoreplication and cell-cycle progression. The photodamage-induced ROS burst aggregates this process (Figures 6 and S6A–S6C). However, the relationship among ptDNA rearrangements, ROS accumulation, and photodamage is complicated. Our results support the idea that ptDNA rearrangements in the plastid genome instability mutant promote ROS production in plastids (Figures 6A–6C), and a previous study supports this (Lepage et al., 2013). Light stimulates ptDNA replication (Oldenburg et al., 2006; Zheng et al., 2011) and can also affect the damage and functional DNA in plastids (Kumar et al., 2014; Oldenburg and Bendich, 2015). In our study, the ptDNA rearrangements of *reca1why1why3* are slightly increased compared with WT under LL conditions, but in GL conditions, this increase is enhanced (Figure 6C), indicating that light may aggravate ptDNA rearrangements in plastid genome instability plants. Both ptDNA rearrangements and ROS accumulation increased in *reca1why1why3* mutant under GL conditions, and a previous study reported ROS triggered by ROS-inducing agents do not induce ptDNA rearrangements (Lepage et al., 2013). We speculate that under GL conditions, the plastid genome instability of *reca1why1why3* mutant is more sensitive to light and substantially accumulates more ptDNA rearrangements, promoting more ROS than the WT compared to LL conditions. Photosynthetic activity is reduced in *reca1why1why3* under GL conditions (Figures 6B, S6A, and S6B), but the difference was diminished between *reca1why1why3* and WT under LL conditions (Figures 6B and S6C). It is possible that photodamage in GL can aggregate the ROS burst and ptDNA rearrangements to further reduce photosynthesis, which induced more ROS accumulation in plastid genome instability plants (Figure 6). Thus, photodamage can boost the ROS signal to modulate endoreplication and the expression of cell-cycle genes in the nucleus, which retard plant growth and development (Figures 6 and S6). Furthermore, we observed that a portion of ROS colocalized with a plastid nucleoid protein, PEND, in plastid genome instability plants

(Terasawa and Sato, 2005; Wang et al., 2014; Figure S5C), suggesting the possibility that instable ptDNA in nucleoids can lead to ROS, which may be different from the ROS produced in the photosystem (Waszczak et al., 2018). However, how the short-range ptDNA rearrangements of plastid genome instability induced ROS is not clear and needs further verification.

In *Drosophila*, mitochondria coordinate cell-cycle progression via at least two metabolic signals—ROS and AMP—to retard cell-cycle progression during the G1/S transition (Mandal et al., 2005; Owusu-Ansah et al., 2008). Due to similar characteristics of plastids and mitochondria and since they were both derived from endosymbiosis (Cavalier-Smith, 2013), plastids may use a mechanism similar to that used by mitochondria to coordinate cell-cycle progression. Our study supports that ROS signaling is involved in regulating endoreplication and the cell cycle in *reca1why1why3* plants through decreasing ROS by LL or ascorbic acid treatment (Figures 6 and S6). Therefore, plastid genome instability plants, at least through the ROS signaling pathway, which modulates endoreplication and the cell cycle, coordinated plastid genome stability and nuclear genome integrity. This provides new perspectives on how both the signal originating from plastid genome instability (perhaps resulting from short-range ptDNA rearrangements) and the response in the nucleus (coordination of plastid and nuclear genome stability) enrich plastid retrograde signaling at the genome level. Our findings demonstrate that communication between the plastid and nuclear genomes is important for regulating plant growth and development.

STAR★METHODS

Detailed methods are provided in the online version of this paper and include the following:

- KEY RESOURCES TABLE
- RESOURCE AVAILABILITY
  - Lead Contact
  - Materials Availability
  - Data and Code Availability
- EXPERIMENTAL MODEL AND SUBJECT DETAILS
  - Plant Materials and Growth Conditions
- METHOD DETAILS
  - Seed per Silique Counts
  - Photosynthetic Parameter Measurements and Pigment Analysis
  - *In Situ* Detection of ROS
  - Trypan Blue Staining
  - Comet Assay
  - qPCR and Detection of DNA Rearrangements by PCR
  - Scanning Electron Microscopy
  - Differential Interference Contrast Light Microscopy
  - Flow Cytometry
  - ChIP
- QUANTIFICATION AND STATISTICAL ANALYSIS

SUPPLEMENTAL INFORMATION

Supplemental Information can be found online at https://doi.org/10.1016/j.celrep.2020.108019.

ACKNOWLEDGMENTS

We thank Professor Normand Brisson (Université de Montréal) for providing the *reca1why1why3* mutant seeds. We thank Professor Wei Chi (Chinese Academy of Sciences) for technical support and critical reading of the article and Yonggang Zheng for helpful discussions. We thank Professor Lizhen Tao (South China Agricultural University) for providing the differential interference contrast (DIC) microscope for analysis. This work was supported by the National Natural Science Foundation of China (grant nos. 31970261, 31425003, and 31770260), the "Ten Thousand People Plan" Leading Talents of Technological Innovation (W03020608), the Top Young Talents (W02070129), the Talent Support Project of Guangdong (2019TQ05N182), and the National Science and Technology Major Project Foundation of China (grant no. 2016ZX08009003-005-005).

AUTHOR CONTRIBUTIONS

H.-B.W. and H.-L.J. conceived the project. S.D. and H.-L.J. performed most of the experiments. L.H. and B.D. made some constructs and performed mutant screening and qPCR measurements. S.D., H.-L.J., and H.-B.W. wrote the manuscript.

DECLARATION OF INTERESTS

The authors declare no competing interests.

Received: March 4, 2019
Revised: April 8, 2020
Accepted: July 20, 2020
Published: August 11, 2020

REFERENCES

Adachi, S., Minamisawa, K., Okushima, Y., Inagaki, S., Yoshiyama, K., Kondou, Y., Kaminuma, E., Kawashima, M., Toyoda, T., Matsui, M., et al. (2011). Programmed induction of endoreduplication by DNA double-strand breaks in *Arabidopsis*. Proc. Natl. Acad. Sci. USA *108*, 10004–10009.

Aguilera, A., and García-Muse, T. (2013). Causes of genome instability. Annu. Rev. Genet. *47*, 1–32.

Boruc, J., Van den Daele, H., Hollunder, J., Rombauts, S., Mylle, E., Hilson, P., Inzé, D., De Veylder, L., and Russinova, E. (2010). Functional modules in the *Arabidopsis* core cell cycle binary protein-protein interaction network. Plant Cell *22*, 1264–1280.

Breuer, C., Braidwood, L., and Sugimoto, K. (2014). Endocycling in the path of plant development. Curr. Opin. Plant Biol. *17*, 78–85.

Cavalier-Smith, T. (2013). Symbiogenesis: Mechanisms, Evolutionary Consequences, and Systematic Implications. Annu. Rev. Ecol. Evol. Syst. *44*, 145.

Chan, K.X., Phua, S.Y., Crisp, P., McQuinn, R., and Pogson, B.J. (2016). Learning the Languages of the Chloroplast: Retrograde Signaling and Beyond. Annu. Rev. Plant Biol. *67*, 25–53.

Chen, P., Sjogren, C.A., Larsen, P.B., and Schnittger, A. (2019). A multi-level response to DNA damage induced by aluminium. Plant J. *98*, 479–491.

Chi, W., Sun, X., and Zhang, L. (2013). Intracellular signaling from plastid to nucleus. Annu. Rev. Plant Biol. *64*, 559–582.

Churchman, M.L., Brown, M.L., Kato, N., Kirik, V., Hülskamp, M., Inzé, D., De Veylder, L., Walker, J.D., Zheng, Z., Oppenheimer, D.G., et al. (2006). SIAMESE, a plant-specific cell cycle regulator, controls endoreplication onset in *Arabidopsis thaliana*. Plant Cell *18*, 3145–3157.

De Veylder, L., Joubès, J., and Inzé, D. (2003). Plant cell cycle transitions. Curr. Opin. Plant Biol. *6*, 536–543.

De Veylder, L., Larkin, J.C., and Schnittger, A. (2011). Molecular control and function of endoreplication in development and physiology. Trends Plant Sci. *16*, 624–634.

Domenichini, S., Benhamed, M., De Jaeger, G., Van De Slijke, E., Blanchet, S., Bourge, M., De Veylder, L., Bergounioux, C., and Raynaud, C. (2012). Evidence for a role of *Arabidopsis* CDT1 proteins in gametophyte development and maintenance of genome integrity. Plant Cell *24*, 2779–2791.

Evans-Roberts, K.M., Mitchenall, L.A., Wall, M.K., Leroux, J., Mylne, J.S., and Maxwell, A. (2016). DNA Gyrase Is the Target for the Quinolone Drug Ciprofloxacin in *Arabidopsis* thaliana. J. Biol. Chem. *291*, 3136–3144.

Fang, X., Zhao, G., Zhang, S., Li, Y., Gu, H., Li, Y., Zhao, Q., and Qi, Y. (2018). Chloroplast-to-Nucleus Signaling Regulates MicroRNA Biogenesis in Arabidopsis. Dev. Cell. *48*, 371–382.e4.

Fox, D.T., and Duronio, R.J. (2013). Endoreplication and polyploidy: insights into development and disease. Development *140*, 3–12.

Golczyk, H., Greiner, S., Wanner, G., Weihe, A., Bock, R., Börner, T., and Herrmann, R.G. (2014). Chloroplast DNA in mature and senescing leaves: a reappraisal. Plant Cell *26*, 847–854.

Green, B.R. (2011). Chloroplast genomes of photosynthetic eukaryotes. Plant J. *66*, 34–44.

Gutierrez, C. (2009). The *Arabidopsis* cell division cycle. Arabidopsis Book *7*, e0120.

Hardy, C.D., and Cozzarelli, N.R. (2003). Alteration of Escherichia coli topoisomerase IV to novobiocin resistance. Antimicrob. Agents Chemother. *47*, 941–947.

Hemerly, A., Bergounioux, C., Van Montagu, M., Inzé, D., and Ferreira, P. (1992). Genes regulating the plant cell cycle: isolation of a mitotic-like cyclin from Arabidopsis thaliana. Proc. Natl. Acad. Sci. USA *89*, 3295–3299.

Horvath, B.M., Kourova, H., Nagy, S., Nemeth, E., Magyar, Z., Papdi, C., Ahmad, Z., Sanchez-Perez, G.F., Perilli, S., Blilou, I., et al. (2017). *Arabidopsis* RETINOBLASTOMA RELATED directly regulates DNA damage responses through functions beyond cell cycle control. EMBO J. *36*, 1261–1278.

Hu, Z., Cools, T., and De Veylder, L. (2016). Mechanisms Used by Plants to Cope with DNA Damage. Annu. Rev. Plant Biol. *67*, 439–462.

Hudik, E., Yoshioka, Y., Domenichini, S., Bourge, M., Soubigout-Taconnat, L., Mazubert, C., Yi, D., Bujaldon, S., Hayashi, H., De Veylder, L., et al. (2014). Chloroplast dysfunction causes multiple defects in cell cycle progression in the *Arabidopsis* crumpled leaf mutant. Plant Physiol. *166*, 152–167.

Inzé, D., and De Veylder, L. (2006). Cell cycle regulation in plant development. Annu. Rev. Genet. *40*, 77–105.

Jin, H., Liu, B., Luo, L., Feng, D., Wang, P., Liu, J., Da, Q., He, Y., Qi, K., Wang, J., and Wang, H.B. (2014). HYPERSENSITIVE TO HIGH LIGHT1 interacts with LOW QUANTUM YIELD OF PHOTOSYSTEM II1 and functions in protection of photosystem II from photodamage in *Arabidopsis*. Plant Cell *26*, 1213–1229.

Jin, H., Fu, M., Duan, Z., Duan, S., Li, M., Dong, X., Liu, B., Feng, D., Wang, J., Peng, L., and Wang, H.B. (2018). LOW PHOTOSYNTHETIC EFFICIENCY 1 is required for light-regulated photosystem II biogenesis in *Arabidopsis*. Proc. Natl. Acad. Sci. USA *115*, E6075–E6084.

Kakizaki, T., Matsumura, H., Nakayama, K., Che, F.S., Terauchi, R., and Inaba, T. (2009). Coordination of plastid protein import and nuclear gene expression by plastid-to-nucleus retrograde signaling. Plant Physiol. *151*, 1339–1353.

Kawai-Yamada, M., Ohori, Y., and Uchimiya, H. (2004). Dissection of *Arabidopsis* Bax inhibitor-1 suppressing Bax-, hydrogen peroxide-, and salicylic acid-induced cell death. Plant Cell *16*, 21–32.

Kimura, S., and Sakaguchi, K. (2006). DNA repair in plants. Chem. Rev. *106*, 753–766.

Kobayashi, Y., Kanesaki, Y., Tanaka, A., Kuroiwa, H., Kuroiwa, T., and Tanaka, K. (2009). Tetrapyrrole signal as a cell-cycle coordinator from organelle to nuclear DNA replication in plant cells. Proc. Natl. Acad. Sci. USA *106*, 803–807.

Kobayashi, Y., Imamura, S., Hanaoka, M., and Tanaka, K. (2011). A tetrapyrrole-regulated ubiquitin ligase controls algal nuclear DNA replication. Nat. Cell Biol. *13*, 483–487.

Kumar, R.A., Oldenburg, D.J., and Bendich, A.J. (2014). Changes in DNA damage, molecular integrity, and copy number for plastid DNA and mitochondrial DNA during maize development. J. Exp. Bot. *65*, 6425–6439.

Kumar, N., Harashima, H., Kalve, S., Bramsiepe, J., Wang, K., Sizani, B.L., Bertrand, L.L., Johnson, M.C., Faulk, C., Dale, R., et al. (2015). Functional Conservation in the SIAMESE-RELATED Family of Cyclin-Dependent Kinase Inhibitors in Land Plants. Plant Cell *27*, 3065–3080.

Kurzbauer, M.T., Pradillo, M., Kerzendorfer, C., Sims, J., Ladurner, R., Oliver, C., Janisiw, M.P., Mosiolek, M., Schweizer, D., Copenhaver, G.P., and Schlögelhofer, P. (2018). *Arabidopsis thaliana* FANCD2 Promotes Meiotic Crossover Formation. Plant Cell *30*, 415–428.

Lepage, É., Zampini, É., and Brisson, N. (2013). Plastid genome instability leads to reactive oxygen species production and plastid-to-nucleus retrograde signaling in *Arabidopsis*. Plant Physiol. *163*, 867–881.

Li, W., Ruf, S., and Bock, R. (2006). Constancy of organellar genome copy numbers during leaf development and senescence in higher plants. Mol. Genet. Genomics *275*, 185–192.

Li, Z., Wakao, S., Fischer, B.B., and Niyogi, K.K. (2009). Sensing and responding to excess light. Annu. Rev. Plant Biol. *60*, 239–260.

Lichtenthaler, H.K., Babani, F., Navrátil, M., and Buschmann, C. (2013). Chlorophyll fluorescence kinetics, photosynthetic activity, and pigment composition of blue-shade and half-shade leaves as compared to sun and shade leaves of different trees. Photosynth. Res. *117*, 355–366.

Liu, J., Chen, S., Chen, L., Zhou, Q., Wang, M., Feng, D., Li, J.F., Wang, J., Wang, H.B., and Liu, B. (2017). BIK1 cooperates with BAK1 to regulate constitutive immunity and cell death in *Arabidopsis*. J. Integr. Plant Biol. *59*, 234–239.

Lukowitz, W., Gillmor, C.S., and Scheible, W.R. (2000). Positional cloning in *Arabidopsis*. Why it feels good to have a genome initiative working for you. Plant Physiol. *123*, 795–805.

Mandal, S., Guptan, P., Owusu-Ansah, E., and Banerjee, U. (2005). Mitochondrial regulation of cell cycle progression during development as revealed by the tenured mutation in Drosophila. Dev. Cell *9*, 843–854.

Maréchal, A., Parent, J.S., Véronneau-Lafortune, F., Joyeux, A., Lang, B.F., and Brisson, N. (2009). Whirly proteins maintain plastid genome stability in *Arabidopsis*. Proc. Natl. Acad. Sci. USA *106*, 14693–14698.

Mochizuki, N., Brusslan, J.A., Larkin, R., Nagatani, A., and Chory, J. (2001). *Arabidopsis* genomes uncoupled 5 (GUN5) mutant reveals the involvement of Mg-chelatase H subunit in plastid-to-nucleus signal transduction. Proc. Natl. Acad. Sci. USA *98*, 2053–2058.

Ni, D.A., Sozzani, R., Blanchet, S., Domenichini, S., Reuzeau, C., Cella, R., Bergounioux, C., and Raynaud, C. (2009). The *Arabidopsis* MCM2 gene is essential to embryo development and its over-expression alters root meristem function. New Phytol. *184*, 311–322.

Odom, O.W., Baek, K.H., Dani, R.N., and Herrin, D.L. (2008). Chlamydomonas chloroplasts can use short dispersed repeats and multiple pathways to repair a double-strand break in the genome. Plant J. *53*, 842–853.

Ogita, N., Okushima, Y., Tokizawa, M., Yamamoto, Y.Y., Tanaka, M., Seki, M., Makita, Y., Matsui, M., Okamoto-Yoshiyama, K., Sakamoto, T., et al. (2018). Identifying the target genes of SUPPRESSOR OF GAMMA RESPONSE 1, a master transcription factor controlling DNA damage response in *Arabidopsis*. Plant J. *94*, 439–453.

Oldenburg, D.J., and Bendich, A.J. (2015). DNA maintenance in plastids and mitochondria of plants. Front. Plant Sci. *6*, 883.

Oldenburg, D.J., Rowan, B.A., Zhao, L., Walcher, C.L., Schleh, M., and Bendich, A.J. (2006). Loss or retention of chloroplast DNA in maize seedlings is affected by both light and genotype. Planta *225*, 41–55.

Owusu-Ansah, E., Yavari, A., Mandal, S., and Banerjee, U. (2008). Distinct mitochondrial retrograde signals control the G1-S cell cycle checkpoint. Nat. Genet. *40*, 356–361.

Parent, J.S., Lepage, E., and Brisson, N. (2011). Divergent roles for the two PolI-like organelle DNA polymerases of *Arabidopsis*. Plant Physiol. *156*, 254–262.

Pedroza-García, J.A., Domenichini, S., Bergounioux, C., Benhamed, M., and Raynaud, C. (2016). Chloroplasts around the plant cell cycle. Curr. Opin. Plant Biol. *34*, 107–113.

Pedroza-García, J.A., Mazubert, C., Del Olmo, I., Bourge, M., Domenichini, S., Bounon, R., Tariq, Z., Delannoy, E., Piñeiro, M., Jarillo, J.A., et al. (2017). Function of the plant DNA polymerase epsilon in replicative stress sensing, a genetic analysis. Plant Physiol. *173*, 1735–1749.

Petrillo, E., Godoy Herz, M.A., Fuchs, A., Reifer, D., Fuller, J., Yanovsky, M.J., Simpson, C., Brown, J.W., Barta, A., Kalyna, M., and Kornblihtt, A.R. (2014). A chloroplast retrograde signal regulates nuclear alternative splicing. Science *344*, 427–430.

Roach, T., and Krieger-Liszkay, A. (2014). Regulation of photosynthetic electron transport and photoinhibition. Curr. Protein Pept. Sci. *15*, 351–362.

Rossel, J.B., Wilson, P.B., Hussain, D., Woo, N.S., Gordon, M.J., Mewett, O.P., Howell, K.A., Whelan, J., Kazan, K., and Pogson, B.J. (2007). Systemic and intracellular responses to photooxidative stress in *Arabidopsis*. Plant Cell *19*, 4091–4110.

Rowan, B.A., Oldenburg, D.J., and Bendich, A.J. (2010). RecA maintains the integrity of chloroplast DNA molecules in *Arabidopsis*. J. Exp. Bot. *61*, 2575–2588.

Saleh, A., Alvarez-Venegas, R., and Avramova, Z. (2008). An efficient chromatin immunoprecipitation (ChIP) protocol for studying histone modifications in *Arabidopsis* plants. Nat. Protoc. *3*, 1018–1025.

Sanchez, M.D., Costas, C., Sequeira-Mendes, J., and Gutierrez, C. (2012). Regulating DNA Replication in Plants. Csh Perspect Biol. *4*, 12.

Shultz, R.W., Lee, T.J., Allen, G.C., Thompson, W.F., and Hanley-Bowdoin, L. (2009). Dynamic localization of the DNA replication proteins MCM5 and MCM7 in plants. Plant Physiol. *150*, 658–669.

Šimková, K., Kim, C., Gacek, K., Baruah, A., Laloi, C., and Apel, K. (2012). The chloroplast division mutant caa33 of *Arabidopsis* thaliana reveals the crucial impact of chloroplast homeostasis on stress acclimation and retrograde plastid-to-nucleus signaling. Plant J. *69*, 701–712.

Sjogren, C.A., Bolaris, S.C., and Larsen, P.B. (2015). Aluminum-dependent terminal differentiation of the *arabidopsis* root tip is mediated through an ATR-, ALT2-, and SOG1-regulated transcriptional response. Plant Cell *27*, 2501–2515.

Sliwinska, E., Mathur, J., and Bewley, J.D. (2012). Synchronously developing collet hairs in *Arabidopsis* thaliana provide an easily accessible system for studying nuclear movement and endoreduplication. J. Exp. Bot. *63*, 4165–4178.

Terasawa, K., and Sato, N. (2005). Visualization of plastid nucleoids in situ using the PEND-GFP fusion protein. Plant Cell Physiol. *46*, 649–660.

Vanacker, H., Carver, T.L., and Foyer, C.H. (2000). Early $H_{(2)}O_{(2)}$ accumulation in mesophyll cells leads to induction of glutathione during the hyper-sensitive response in the barley-powdery mildew interaction. Plant Physiol. *123*, 1289–1300.

Wang, P., Liu, J., Liu, B., Da, Q., Feng, D., Su, J., Zhang, Y., Wang, J., and Wang, H.B. (2014). Ferredoxin:thioredoxin reductase is required for proper chloroplast development and is involved in the regulation of plastid gene expression in *Arabidopsis thaliana*. Mol. Plant *7*, 1586–1590.

Waszczak, C., Carmody, M., and Kangasjärvi, J. (2018). Reactive oxygen species in plant signaling. Annu. Rev. Plant Biol. *69*, 209–236.

Weimer, A.K., Biedermann, S., Harashima, H., Roodbarkelari, F., Takahashi, N., Foreman, J., Guan, Y., Pochon, G., Heese, M., Van Damme, D., et al. (2016). The plant-specific CDKB1-CYCB1 complex mediates homologous recombination repair in *Arabidopsis*. EMBO J. *35*, 2068–2086.

Woodson, J.D., and Chory, J. (2008). Coordination of gene expression between organellar and nuclear genomes. Nat. Rev. Genet. *9*, 383–395.

Woodson, J.D., Perez-Ruiz, J.M., and Chory, J. (2011). Heme synthesis by plastid ferrochelatase I regulates nuclear gene expression in plants. Curr. Biol. *21*, 897–903.

Yao, N., and Greenberg, J.T. (2006). *Arabidopsis* ACCELERATED CELL DEATH2 modulates programmed cell death. Plant Cell *18*, 397–411.

Yi, D., Alvim Kamei, C.L., Cools, T., Vanderauwera, S., Takahashi, N., Okushima, Y., Eekhout, T., Yoshiyama, K.O., Larkin, J., Van den Daele, H., et al. (2014). The *Arabidopsis* SIAMESE-RELATED cyclin-dependent kinase inhibitors SMR5 and SMR7 regulate the DNA damage checkpoint in response to reactive oxygen species. Plant Cell *26*, 296–309.

Yin, H., Zhang, X., Liu, J., Wang, Y., He, J., Yang, T., Hong, X., Yang, Q., and Gong, Z. (2009). Epigenetic regulation, somatic homologous recombination, and abscisic acid signaling are influenced by DNA polymerase epsilon mutation in *Arabidopsis*. Plant Cell *21*, 386–402.

Yoshiyama, K.O. (2016). SOG1: a master regulator of the DNA damage response in plants. Genes Genet. Syst. *90*, 209–216.

Yoshiyama, K., Conklin, P.A., Huefner, N.D., and Britt, A.B. (2009). Suppressor of gamma response 1 (SOG1) encodes a putative transcription factor governing multiple responses to DNA damage. Proc. Natl. Acad. Sci. USA *106*, 12843–12848.

Yoshiyama, K.O., Kobayashi, J., Ogita, N., Ueda, M., Kimura, S., Maki, H., and Umeda, M. (2013). ATM-mediated phosphorylation of SOG1 is essential for the DNA damage response in *Arabidopsis*. EMBO Rep. *14*, 817–822.

Yoshiyama, K.O., Kaminoyama, K., Sakamoto, T., and Kimura, S. (2017). Increased Phosphorylation of Ser-Gln Sites on SUPPRESSOR OF GAMMA RESPONSE1 Strengthens the DNA Damage Response in *Arabidopsis thaliana*. Plant Cell *29*, 3255–3268.

Zampini, É., Lepage, É., Tremblay-Belzile, S., Truche, S., and Brisson, N. (2015). Organelle DNA rearrangement mapping reveals U-turn-like inversions as a major source of genomic instability in *Arabidopsis* and humans. Genome Res. *25*, 645–654.

Zeng, L., Gu, Z., Xu, M., Zhao, N., Zhu, W., Yonezawa, T., Liu, T., Qiong, L., Tersing, T., and Xu, L. (2017). Discovery of a high-altitude ecotype and ancient lineage of *Arabidopsis thaliana* from Tibet. Sci. Bull. (Beijing) *62*, 1628–1630.

Zheng, Q., Oldenburg, D.J., and Bendich, A.J. (2011). Independent effects of leaf growth and light on the development of the plastid and its DNA content in Zea species. J. Exp. Bot. *62*, 2715–2730.

STAR★METHODS

KEY RESOURCES TABLE

REAGENT or RESOURCE	SOURCE	IDENTIFIER
Antibodies		
Mouse Anti-FLAG M2 affinity Gel	Sigma	Cat# A2220; RRID: AB_10063035
Bacterial and Virus Strains		
Escherichia coli strain DH5a	TaKaRa	Cat# 9057
Chemicals, Peptides, and Recombinant Proteins		
ciprofloxacin	Sigma	Cat# 17850; RRID:101674139
novobiocin	newprobe	Cat# P006577
Hydrogen peroxide	Sigma	Cat# 323381; RRID: 102033624
diaminobenzidine (DAB)	newprobe	Cat# PB10214-1
Nitro blue tetrazolium (NBT)	newprobe	Cat# PB10519-2
CM-H_2DCFDA	Invitrogen	Cat# C6827; RRID: 2049036
ascorbic acid	newprobe	Cat# PB10094
DAPI	Sigma	Cat# D8417
Trypan Blue	Sigma	Cat# 93595
Critical Commercial Assays		
Prime Script RT Reagent Kit	TaKaRa	Cat# RR047A
SYBR Premix Ex Taq	TaKaRa	Cat# RR420A
Comet Assay Kit	Trevigen	Cat# 4250-050-K
Deposited Data		
DNA sequencing data	This paper	Accession Number: SRP268535
Experimental Models: Organisms/Strains		
Arabidopsis thaliana: Col-0 wild-type	This paper	N/A
Arabidopsis thaliana: Tibet-0	Zeng et al., 2017	N/A
Arabidopsis thaliana: Landsberg erecta	This paper	N/A
Arabidopsis thaliana: *reca1why1why3*	Zampini et al., 2015	N/A
Arabidopsis thaliana: *smr7*	NASC	N628496
Arabidopsis thaliana: *smr7reca1why1why3*	This paper	N/A
Arabidopsis thaliana: *lpe1-3*	Jin et al., 2018	N/A
Arabidopsis thaliana: *gun5*	Mochizuki et al., 2001	N/A
Arabidopsis thaliana: *why1*	NASC	N599937
Arabidopsis thaliana: *why3*	NASC	N667694
Arabidopsis thaliana: *reca1-1*	NASC	N666139
Arabidopsis thaliana: *sog1-1*	Ogita et al., 2018	N/A
Arabidopsis thaliana sog1-101	Ogita et al., 2018	N/A
Oligonucleotides		
Primers for qPCR, see Table S1	This paper	N/A
Primers for mutant identification, see Table S1	This paper	N/A
Primers for ptDNA arrangement, see Table S1	This paper	N/A
Primers for ChIP-qPCR, see Table S1	This paper	N/A
Primers for vectors construction, see Table S1	This paper	N/A

(*Continued on next page*)

Continued

REAGENT or RESOURCE	SOURCE	IDENTIFIER
Recombinant DNA		
35S::SOG1-FLAG (pHBT)	This paper	N/A
35S::PEND-CFP	Wang et al., 2014	N/A
Software and Algorithms		
Prism 6	GraphPad	https://www.graphpad.com/
ImageJ	NIH	https://imagej.net/Welcome
CASP comet assay software	http://casplab.com/	http://casplab.com/

RESOURCE AVAILABILITY

Lead Contact

Further information and requests for resources and reagents should be directed to and will be fulfilled by the Lead Contact, Hong-Bin Wang (wanghongbin@gzucm.edu.cn).

Materials Availability

Materials will be provided upon request to Lead Contact.

Data and Code Availability

The sequencing raw data relating to Figure S2B have been submitted to the NCBI Sequence Read Archive (SRA; http://www.ncbi.nlm.nih.gov/sra) under accession number SRP268535 (Col-0: SRR12077407; SRR12077408; SRR12077409, *reca1why1why3*: SRR12077404; SRR12077405; SRR12077406).

EXPERIMENTAL MODEL AND SUBJECT DETAILS

Plant Materials and Growth Conditions

Arabidopsis thaliana ecotype Columbia-0 (Col-0) was used as the wild-type (WT, control). *Arabidopsis thaliana* ecotype Tibet-0 (Zeng et al., 2017) and Landsberg erecta were also used in this study. The *reca1why1why3* triple mutant (*reca1-1:* SALK_057982; *why1*: SALK_099937; *why3*: W138*, the TGG codon 138 was changed to a TGA stop codon) was described previously (Zampini et al., 2015). Cell cycle-related mutants *smr7* (N628496) and *reca1-1* (N666139), *why1* (N599937), *why3* (N667694), which are impaired in factors involved in maintaining plastid genome stability. The *sog1-1* and *sog1-101* mutants were described previously (Ogita et al., 2018). The *gun5* mutant was described previously (Mochizuki et al., 2001). Homozygous lines were selected by PCR, and gene expression was analyzed by qPCR; the primers used are listed in Table S1. The quadruple mutant *smr7reca1why1why3 was* obtained through crossing the *smr7* with the *reca1why1why3* mutant. The method for genetic background of *smr7reca1why1why3* mutants were confirmed as previous report (Lukowitz et al., 2000) (Figure S3D). Plants were grown in soil in a growth chamber under 100 μmol photons m^{-2} s^{-1}, 12 h light/12 h dark photoperiod, 21°C and 60% relative humidity. For CIP and NOV treatments, plants were grown on ½ MS medium with the respective reagent for 14 days. For H_2O_2 treatments, plants were grown on ½ MS medium with the respective reagent for 7 days.

METHOD DETAILS

Seed per Silique Counts

Seed fertility analysis was performed as described previously (Kurzbauer et al., 2018). Mature but still green siliques originating from the fifth to the thirtieth flower per stem were harvested and incubated in 95% ethanol at room temperature for 1 to 3 days for destaining. The ethanol was exchanged several times until the tissue was destained, and seeds inside the siliques were counted manually under a dissection microscope.

Photosynthetic Parameter Measurements and Pigment Analysis

After 20 min of dark adaptation, chlorophyll fluorescence parameters were measured with the MAXI version of the Imaging-PAM M-Series chlorophyll fluorescence system (Heinz-Walz Instruments), using the conditions described previously (Jin et al., 2014). The F_o and F_m values were initially determined, followed by a 715 s delay, which was in turn followed by a 60 s actinic light treatment (100 μmol photons $m^{-2}s^{-1}$) involving 36 saturation pulses (2,800 μmol photons $m^{-2}s^{-1}$) applied at 20 s intervals. Excitation pressure was recorded to determine the maximum photochemical efficiency of PSII (F_v/F_m), NPQ, qP. Light-response curves of Φ_{PSII} and ETR were determined at light intensities of 0, 81, 145, 186, 281, 335, 461, 701 and 926 μmol photons $m^{-2}s^{-1}$. The duration of illumination

at individual light intensities was 3 min; after 3 min of illumination, a saturation pulse was applied. Chlorophyll was extracted from 25-day-old plants using 80% acetone in 2.5 mM HEPES-KOH, pH 7.5, and chlorophyll levels were determined as described previously (Lichtenthaler et al., 2013).

In Situ Detection of ROS

Hydrogen peroxide (H_2O_2) and superoxide (O^{2-}) were detected using DAB and NBT staining, respectively, as previously described (Kawai-Yamada et al., 2004; Vanacker et al., 2000). Whole plants were vacuum infiltrated in 0.1% NBT (in 10 mM potassium phosphate buffer, pH 7.8) or 5 mM DAB-HCl, pH 3.8. NBT staining was performed in the dark for 1 h at room temperature, and DAB was incubated under growth light intensity conditions (100 μmol photons m^{-2} s^{-1}) for 3 h. Stained leaves were boiled in acetic acid/glycerol/ethanol (1:1:3 [v/v/v]) for 10 min. Plants grown under GL conditions were photographed with a camera.

Protoplasts were isolated from 14-day-old seedlings and stained with CM-H_2DCFDA to detect ROS as described previously (Yao and Greenberg, 2006). The signals were observed by confocal laser-scanning microscopy (Zeiss LSM 880). CFP signals were visualized with excitation at 458 nm (emission: 475 nm), CM-H_2DCFDA signals were visualized with excitation at 488 nm (emission: 525 to 535 nm), and chloroplast autofluorescence (488-nm excitation) was visualized at 738 to 793 nm.

Trypan Blue Staining

Trypan blue staining was performed as previously described (Liu et al., 2017), using 0.01% trypan blue solution prepared in lactophenol solution (phenol/lactic acid/glycerol/water, 1:1:1:1, [v/v/v/v]). Leaves from 25-day-old plants were boiled in staining solution for 10 min. After cooling, the leaves were destained in chloral hydrate solution (chloral hydrate/glycerol/water, 4:1:2, [m/v/v]). Images were captured under a Zeiss stereomicroscope (SteREO Lumar.V12).

Comet Assay

Protoplasts from 14-day-old seedlings were used to perform the alkaline comet assay with a Comet Assay Kit from Trevigen (CAT#4250-050-K). SYBR Gold from Life Technologies was used for comet staining. Comets were captured under a Zeiss LSM 880 confocal microscope with excitation/emission wavelengths of 488 nm/505 to 530 nm and analyzed using the Comet Assay Software Project package.

qPCR and Detection of DNA Rearrangements by PCR

Total RNA was extracted from frozen *Arabidopsis* tissues or fresh rosette leaves using a RNeasy Plant Mini Kit (QIAGEN). RNA samples were reverse-transcribed into first-strand cDNA using a PrimeScript RT Reagent Kit (Takara). qPCR was performed using gene-specific primers and SYBR Premix ExTaq reagent (Takara) on a real-time RT-PCR System (RoChe-LC480), according to the manufacturer's instructions. Reactions were performed in triplicate for each sample, and gene expression levels were normalized to *ACTIN2*. The primers used are listed in Table S1. To investigate DNA rearrangements, total DNA was isolated from the samples via cetyl trimethylammonium bromide DNA extraction. DNA rearrangements were detected as described previously (Maréchal et al., 2009). The primers used are listed in Table S1.

Scanning Electron Microscopy

The second pair of fresh leaves from 25-day-old plants was fixed in 5% (v/v) glutaraldehyde in PBS buffer, pH 7.4, dehydrated in ethyl alcohol, and dried thoroughly in a CO_2 Critical Point instrument. Epidermal cell was subjected to scanning electron microscopy observation (Hitachi-3400N).

Differential Interference Contrast Light Microscopy

Fully formed but still green Col-0 and *reca1why1why3* siliques were submerged in transparent buffer (chloral hydrate/gum arabic/water/glycerol, 8:7.5:60:5, [m/m/v/v]) overnight until transparent. Subsequently, seeds were extracted from the siliques and observed by Differential interference contrast (DIC) light microscopy (Olympus BX51). Images of seeds were obtained with a CCD camera.

Flow Cytometry

Nuclear DNA content was measured as described previously (Sliwinska et al., 2012). The second pair of leaves from 25-day-old plants or 14-day-old seedlings was chopped in Galbraith buffer (45 mM $MgCl_2$, 30 mM sodium citrate, 0.2% Triton X-100, 20 mM MOPS, 1% PVP-40, 10 mM disodium EDTA dihydrate, and 2% [v/v] β-mercaptoethanol). The extracts were filtered through 48 nm nylon mesh, and released nuclei were stained with 5 μg ml^{-1} 4′,6-diamidino-2-phenylindole (DAPI; Sigma). Ploidy level in 20,000 isolated nuclei was measured by flow cytometry (MoFlo XDP), with a 355 nm UV laser (40 mW) and a 455 nm long-pass emission filter.

ChIP

Chromatin immunoprecipitation (ChIP) experiments were performed as previously described (Saleh et al., 2008) with some modifications: Briefly, 10 mL of *reca1why1why3* or WT protoplasts was transfected with *35S:SOG1-Flag* plasmids (10 mg). After 18 h, the protoplasts were fixed in 1% (v/v) formaldehyde. Glycine was added to a final concentration of 0.125 M to titrate the remaining

formaldehyde. Protoplasts were harvested by centrifugation at 100 *g* for 3 min and resuspended in SDS lysis buffer (50 mM Tris-HCl at pH 7.5, 150 mM NaCl, 1 mM PMSF, 1 mM EDTA, 1% SDS, 1% [v/v] Triton X-100, and 0.1% sodium deoxycholate) following sonication. Anti-FLAG M2 affinity gel (Sigma-Aldrich) was used for each immunoprecipitation, and the enriched DNA fragments were analyzed by qPCR using previously described primers listed in Table S1 (Weimer et al., 2016; Yi et al., 2014). The amount of DNA recovered after ChIP was initially normalized to the total input DNA used for each immunoprecipitation. ChIP signals in *reca1why1-why3* were normalized to those in the WT, which was set to 1.

QUANTIFICATION AND STATISTICAL ANALYSIS

In this study, significant differences between two samples were determined with Two-tailed paired Student's t test. Error bars represent standard error of mean, 'n' represents the sample size, as mentioned in the figure legends. And asterisks indicate the statistical significance: *, $p < 0.05$; **, $p < 0.01$; ***, $p < 0.001$. At least three biological replicates were included. Statistical analysis was performed by GraphPad Prism 6. Leaf area, cell area, cell number were analysis by ImageJ. Comet assay was analysis by CASP comet assay software from http://casplab.com/.